

# Effect of SiC Particles on Fatigue Life of AL-Matrix Composites

Z. Hosseini Tabar, F. Barati\*

Mechanical Engineering Department, Islamic Azad University, Hamedan Branch, Hamedan, Iran.

## Article info

### Article history:

Received 05 August 2019

Received in revised form

07 September 2019

Accepted 16 September 2019

### Keywords:

Fatigue life

Cohesive zone model

Metal matrix composite

Particulate reinforcement

## Abstract

In the present study, a micromechanical modeling approach based on volumetric element was considered from a composite consisted of three components: matrix, particle, and particle-matrix intermediate phase. In order to predict the behavior of the damage evolution in the composite, the particle-matrix intermediate phase was modeled based on the cohesive zone model and disruptive elastoplastic behavior was considered for matrix. In order to study the efficiency of the implemented model, at first, modeling processes were conducted using the USERMAT code in finite element ANSYS software, and then the growth of fatigue damage was investigated in the AL composite reinforced with SiC particles. For this purpose, after the study of characterization static constant of cohesive zone model, validation of the static model was approved. S-N curve obtained from experimental results for pure AL were used for Characterization fatigue constants of the matrix. Comparison of the obtained results from finite element analysis with that of experiment, justifies the capability of the employed model to predict the fatigue life of metal matrix composites reinforced with particles in other conditions and is able to consider the effect of volume fraction in predicting fatigue life while the model benefits from the lowest tests for the characterization constants of model.

## Nomenclature

$\sigma$	Stress	$\epsilon$	Strain
$\gamma$	Shear strain	$\tau$	Shear stress
$R$	Radius of the particles	$V_f$	Volume fraction of the particles
$G_{IC}$	Fracture toughness	$\beta$	The combination mode ratio
$\gamma_m^f$	Shear strain at the end of the damage	$\epsilon_m$	Current effective strain
$h_0$	Interlayer thickness	$C$	Reduced interlayer stiffness matrix
$E_0$	Initial Young's moduli	$G_0$	Initial shear moduli
$D$	Damage	$c$	Empirical constants
$G_c$	Fracture toughness	$\bar{\sigma}$	Hydrostatic stress
$\epsilon_{ij}^*$	Resulting strains	$W_0^D$	Maximum strain energy density
$\sigma_{Ut}^R$	Residual strength at the current moment	$\sigma_{Ut}^0$	Initial tensile strength
$N$	Cycle	$E \& G$	Elastic stiffness
$G_c$	Fracture toughness	$A_d$	Damaged area
$\tau_c$	Strength of the interlayer zone	$l_{cz}$	Identity matrix

\*Corresponding author: F. Barati (Associate Professor)

E-mail address: Farzanbarati@yahoo.com

<http://dx.doi.org/10.22084/jrstan.2019.19829.1102>

ISSN: 2588-2597

$K$	Initial stiffness of the interlayer element	$\varepsilon_n^0$	Normal interlayer strain
$\gamma_{tn}^0$	Out-of-plane shear strains in the interlayer element	$\varepsilon_n^*$	Irreversibility condition associated with damage parameter in the interlayer element
$E$	Young's modulus along the thickness direction	$\Delta W^D$	Changes in the strain (deformation) energy per unit volume
$b$	Length of the crack front (width of the sample)	$m$ & $c$	Constants in Paris' law for crack length growth rate
$A\varepsilon$	Cohesive element area in the interlayer debonding plane	$\varepsilon_m^*$	Maximum effective strain during each loading stage
$\Delta G$	Changes in the strain energy release rate of the cohesive element during the current fatigue cycle	$G_{th}$	Strain energy release rate of the cohesive element on the average of fatigue initiation
		$m$	Empirical constant

## 1. Introduction

Achieving materials with more efficient mechanical properties is of great significance. In addition to paving the way for the development of new productions, manufacturing new materials with higher strength helps optimizing machinery and equipment. Industries' need for lightweight materials of more strength has led to researches on as well as the development of new materials. Under difficult conditions where high strength at high temperatures is required, more researches and studies are to be conducted on the production of metal-based materials. Hence, most of the recent researches on advanced materials have been focused on metal-based composites, which are among the engineering materials capable of meeting the aforementioned requirements.

Amongst metals, after iron and steel, aluminum holds second place in the world market. Rapid growth in the aluminum industry is associated with different, unique properties of aluminum, making it one of the most engineering and structural materials. Although aluminum is lightweight, some of its alloys outperform structural steel in terms of strength. Aluminum exhibits good electrical and thermal conductivity and is a good reflector of light and heat. In most applications, aluminum can highly resist to corrosion and is considered a non-toxic metal. Aluminum can be manufactured or cast into any shape with the various surface finish. Considering all these various properties, it is not surprising aluminum is the first priority among engineering materials [1].

Pure aluminum is fairly soft. In order to deal with this problem, this metal may be combined with other metals (alloying elements) to form alloys. Most aluminum available in the market is alloyed with at least one other element [2]. Aluminum alloy is extensively combined with different ceramic particles as reinforcement, among the most widely used of which silicon carbide may be pointed out.

Hence, these materials inherit metal properties such as flexibility and toughness as well as ceramic properties such as high stiffness (Young's modulus) and high strength [3].

Damages in particle-reinforced metal-matrix composites (PMCs) are associated with changes in the matrix of particles and may occur as 1. fracture of particles, 2. deboning or cracking of the interface between the matrix and particles, and 3. matrix damage caused by merging and growth of microscopic voids or shear processes [4].

Aluminum-based composites provide particular advantages in aerospace and automotive industries as well as other structural applications. Additionally, composite failure due to cyclic loads is considered a major problem in these industries. Hence, the fatigue behavior of these materials is an important factor to be taken into account [5].

Fatigue is the phenomenon in which mechanical properties decline due to cyclic loading. Cyclic loads may be of the mechanical and thermal type or a combination of both. Fatigue behavior of structural materials is usually divided into two stages: 1) Crack nucleation, and 2) Crack Growth [6].

Employing ceramic particle reinforcements of high stiffness can significantly increase the resistance against fatigue. Fatigue resistance in PMMCs depends on many factors including the volume fraction of particles, particle size, microstructure of the matrix and interface, presence of inclusion or defects caused by the production process, and environmental conditions of the experiment [7-11].

Nemati and his coworker (2016) studied the annealed CP-Ti (Grade 2) by Equal Channel Angular Extrusion (ECAE) up to 2 passes at a temperature of 400°C following route A with a constant ram speed of 30mm/min through a die angle of 90° between the die channels. Mechanical properties of the extruded materials were obtained at different strain rates.

The results indicated that the tensile yield stress and ultimate tensile strength of the extruded specimens increased significantly after 2 passes of ECAE process [12].

Madadi and his coworkers in (2018) studied the bond stress in steel reinforcements embedded in concrete containing polymer fibers, micro- and nano-silica particles.

The results indicated that micro and nano-silica particles, compared to fibers, had more impacts on improving the reinforcement-concrete bond strength. Moreover, the highest bond strength was observed for the specimen containing equal content of the micro and nano-silica particle [13].

Majzooobi and his coworkers (2018) studied the Mg-SiC nanocomposite specimens, which were produced at low strain rate of  $8 \times 10^{-3} \text{s}^{-1}$ , using a universal INSTRON testing machine, strain rate of about  $8 \times 10^2 \text{s}^{-1}$  using a drop hammer and at strain rate of about  $1.6 \times 10^3 \text{s}^{-1}$  employing a Split Hopkinson Pressure Bar (SHPB). The results showed an increase in the wear resistance as the nano-reinforcement increased [14].

Although there are a large number of investigation on Al-based composite materials, it seems that there are not sufficient references to deal with the fatigue life of Al-based alloy reinforced by Nano-particles. In designing particle composites, it is necessary to predict the failure behavior under static and fatigue loadings. Deriving a complete model of the components in a structure composed of PMMCs is not computationally cost-efficient. Meanwhile, considering equivalent properties for composites in the approach of continuum mechanics still neglects the interactions and stress concentrations in the locations where particles are connected to the matrix, hence an appropriate prediction of the failure conditions is not provided. In such structures, the use of multi-scale modeling concept can prove very useful. In this approach, first, the effects of particles and matrix on each other is investigated in the form of a unit cell using the concept of micromechanics, and ultimately, the analysis results are generalized to the entire structure through the concept of continuum mechanics. In addition to offering appropriate accuracies, this approach is also computationally cost-efficient. Hence, the same approach was employed in the present study. To this end, first the representative volume element (RVE) of the composite structure was modeled, and then its static and fatigue behaviors were simulated with emphasis on the particle-matrix debonding damage mode. The inter-phase between the matrix and particles was considered in the framework of damage mechanics based on bilinear cohesive zone model (CZM). Determining the properties for the cohesive zone model associated with the inter-phase between the particles and matrix was carried out by matching the experimental results of a silicon carbide reinforced aluminum matrix composite with the aforementioned properties at a specific volume fraction. Then, the fatigue results in this cell were assessed using the experimental micromechanical results.

Finite element implementation of the mentioned model was carried out using the User mat subroutine written in ANSYS software package.

## 2. Micromechanical Modeling Using Representative Volume Element

In the concept of micromechanical modeling using representative volume element (RVE), a unit cell comprised of particles and the adjacent matrix as well as a part of the adjacent particles is modeled, through replication of which the considered composite is created at a given volume fraction of the reinforcement phase. On the two symmetric sides as shown in Figure 1, symmetric boundary conditions were imposed and on the other two sides periodic boundary conditions were imposed. On the plane perpendicular to the Y-axis, the out-of-plane displacement (displacement in Y direction) is zero, i.e. that unit cell is only allowed to deform in the XZ plane. Similarly on the plane perpendicular to the X-axis, displacement in the X direction is zero and the unit cell is allowed to deform in the YZ plane. This means that the unit cell will retain its original cross-section under applied loading in the Z direction. The bottom surface of the unit cell was constrained in all three directions, i.e. zero displacement in x, y, and z direction. The top surface of the idealized unit cell was subject to one of the following types of loading boundary conditions (1) stress controlled consisting of a uniform tensile traction of and (2) strain controlled consisting of displacement compatible with a uniform tensile unit strain.

These simplified boundary conditions were considered because the complex loading conditions at the d-a interface precludes modeling of actual boundary conditions. The complex loading condition at the d-a interface is clear from the stress distributions. In the present study, the mentioned approach was used to investigate the fatigue life of PMCs. In the created model, in order to simulate the particle-matrix debonding failure mode, which is one of the important failure modes in particle composites, three components were considered for the unit cell: 1. matrix, 2. spherical particle, and 3. narrow-thickness interface volume between particle and matrix was considered as a spherical membrane around the particles.

In the present study, the particle shapes were considered spheres and the unit cell was considered a cube with a particle at the center and 6 particles at the center of its 6 faces. In this model, the dimensions of the unit cell were selected so that the volume fraction of the particles within the unit cell equals that of the large-scale composite. Hence, the side length of the cube (a) is obtained using Eq. (1):

$$a = \sqrt[2]{\frac{\left(4 \times \frac{4}{3} \pi R^3\right)}{V_f}} \quad (1)$$

where  $R$  is the radius of the particles and  $V_f$  is the volume fraction of the particles in the composite.

Considering the symmetric shape of the unit cell with respect to the 3 intermediate planes running parallel to the faces, in order to optimize the finite element model, it is sufficient to model one-eighth of the cube, and then apply symmetry boundary conditions to the three planes. The load condition in the present study was considered as a periodic load condition in the Software.

The final finite element model of one-eighth of the cube along with the applied meshing is demonstrated in Fig. 1.

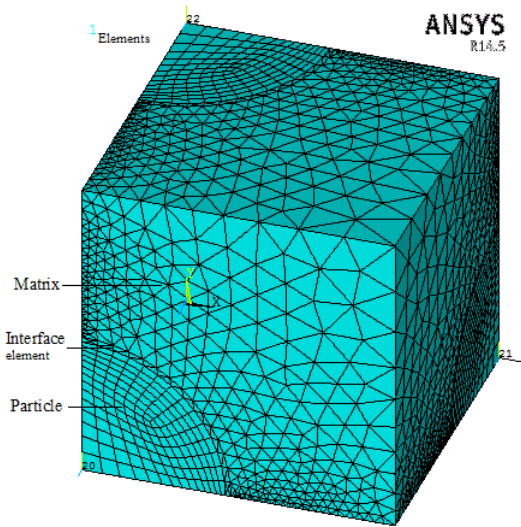


**Fig. 1.** Final FEM element model for the one eighth unit cell of mentioned particulate composite.

### 3. Simulating the Behavior of the Components of the Unit Cell

Isotropic, linear elastic material behavior was used to model the particles. Elasto-plastic behavior was considered for the matrix in order to take into account the plasticity effects, for the failure behavior of which Von-Mises yield criterion was used.

In order to model the static behavior of the matrix, the elastoplastic model available in the ANSYS software package was used. In this study, kinematic stiffening behavior was used during the cyclic loading. This behavior provides more accurate estimations compared to isotropic behavior and takes into account the Bauschinger effect.

Considering its inter-phase nature and stress concentration, the interface volume between particle and matrix was modeled using a cohesive zone model (CZM).

In case of static and fatigue loading, the CZM was implemented into the ANSYS software package using the available subroutine programmed by the user (the user may). It should be noted the code for spherical particles should be written in spherical coordinates, hence the normal direction in the structural relations

is along the radial direction in the local spherical coordinates of each particle. Moreover, each particle's coordinate should match the respective local spherical coordinates.

The interlayer element used in this study was the eight-node solid element with limited-thickness, known as Solid-Like Interlayer Element. The formulation of this element is based on the formulations for isoperimetric hexahedral solid element; however, instead of 6 stress components, 3 interlayer stress components, which are responsible for this phenomenon, are included.

The interface phase between particles and matrix was meshed using Solid185 element, which is compatible with the cohesive element. A schematic of this interlayer element is illustrated in Fig. 2.

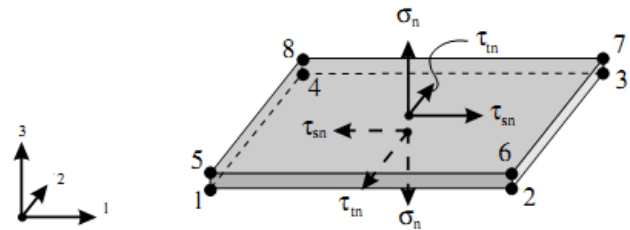


**Fig. 2.** A solid-like interface element [15].

### 4. Cohesive Zone Model

The theory of Linear Elastic Fracture Mechanics (LEFM) is one of the main methods for the analysis of crack growth under brittle fracture conditions, like debonding of the particle from the matrix. Despite its many advantages, the disadvantages of these methods are as follows: First, a singularity is included at the crack tip, which complicates the analysis. Second, an initial crack is required for analysis, meaning that crack initiation in a healthy state of materials may not be predicted.

Employing the Cohesive Zone Model (CZM) can prove useful in order to overcome the limits of fracture mechanics, since use of CZM approach, in addition to tackling the above problems, does not require re-meshing for analysis of crack growth as failure and crack growth is modeled as a gradual decrease in the stiffness of the interlayer element in this approach.

The CZM model is based on presenting a softening structural relation for the damaged zone around the crack tip. The mechanism of this method for the bilinear model is shown in Fig. 3.

According to Fig. 3, the relationship between stress and strain (displacement) in the interlayer element is initially of linear elastic type. Upon reaching a maximum value, which is the interlayer strength under the respective modal ratio conditions, the gradual decrease in the element stiffness is initiated, approaching zero until complete failure.

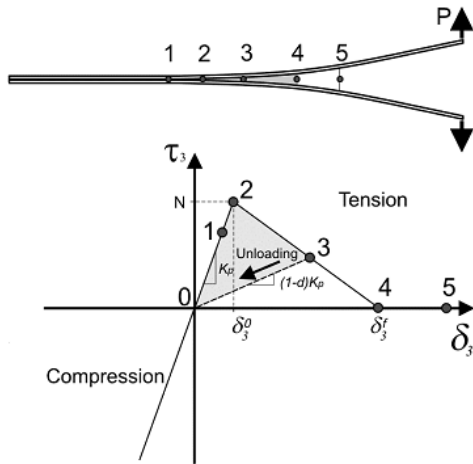


**Fig. 3.** Cohesive zone ahead of delamination tip and Bi-linear constitutive equation [16].

Damage variable is defined as the ratio of stiffness decrease to the initial stiffness at each strain state. This parameter represents the damage growth in the interlayer element and may assume values from 0 to 1. The parameter assumes the value of zero if the interlayer element is located within the elastic region of the structural relation, meaning that the elastic stiffness of the element is equal to its initial value. As the strain increases and reaches the damage initiation point, the element enters the softening stage of the structural relation, increasing the value of the damage variable as Young’s modulus of the element decreases. As the strains in the element increase to reach its ultimate point, the value of this parameter approaches 1; consequently, Young’s modulus decreases as well as the (tensile) stress of the element until the zero value are reached. As a result, the crack grows as long as the length of the element, and new crack areas are formed. It should be noted that at each strain state, loading and unloading occurs along the elastic line with the current stiffness. However, since normal compressive stress does not affect crack growth, it is usually assumed the corresponding stiffness decrease is not applied.

## 5. Simulating Particle Debonding from Matrix under Static Loading:

### 5.1. Structural Relations of Cohesive Element

Balzani and Wagner (2008) presented a powerful solid-like interlayer element based on CZM for modeling the interlayer debonding in layered composite materials under combined loading [15].

In the present research, the cohesive interlayer element used for static loading was based on the structural models presented by Bao and his coworkers [29], which are explained in the following lines.

According to Fig. 3, under any loading mode, the

damage is initiated at the point where the stress in the elastic interlayer element has reached its ultimate value. Hence, regarding this definition, the corresponding strains of the damage initiation point, based on the strength of the respective pure modes, are defined according to Eq. (2):

$$\varepsilon_n^0 = \frac{\sigma_n^U}{K}, \quad \gamma_{3n}^0 = \frac{\tau_{3n}^U}{K}, \quad \gamma_{tn}^0 = \frac{\tau_{tn}^u}{K} \quad (2)$$

where  $K$  is the initial stiffness of the interlayer element in the stress-strain space,  $\varepsilon_n^0$  represents the normal interlayer strain, and  $\gamma_{3n}^0$  and  $\gamma_{tn}^0$  indicate the out-of-plane shear strains in the interlayer element corresponding to the damage initiation point.

In modeling the interlayer debonding growth through CZM, according to Griffith theory, the required energy for the destruction of elements and crack growth, i.e. the area bounded by the graph of structural relationships in the stress-displacement space, equals the critical strain energy release rate (fracture toughness) of the respective loading mode [17].

Hence, according to Fig. 3 as well as the bilinear stress-strain relation of the interlayer zone, the ultimate strain corresponding to the fracture of the interlayer element in each pure mode is obtained using Eq. (3):

$$\varepsilon_n^f = \frac{2G_{Ic}}{h_0\sigma_n^0}, \quad \gamma_{sn}^f = \frac{2G_{IIc}}{h_0\tau_{sn}^0}, \quad \gamma_{tn}^f = \frac{2G_{IIIc}}{h_0\tau_{tn}^0} \quad (3)$$

where  $h_0$  is the interlayer thickness, and  $G_{Ic}$ ,  $G_{IIc}$ , and  $G_{IIIc}$  represent the fracture toughness corresponding to single loading modes I, II, and III, respectively. Since in most structures, crack initiation and growth are much more likely to occur under combined modes than single modes, development of an interlayer formulation for combined loading modes is inevitable.

In the employed formulation of this research, Young’s modulus of the interlayer element for all loading modes was considered similar. Moreover, the ultimate strength in shear modes was also considered equal, i.e.  $\tau_{tn}^0 = \tau_{sn}^0 = \tau^0$ .

In order to present the formulation of the structural relation for combined loading modes, effective strain parameter is defined as Eq. (4):

$$\varepsilon_m = \sqrt{\langle \varepsilon_n \rangle^2 + \gamma_{sn}^2 + \gamma_{tn}^2} \quad (4)$$

where the operator  $\langle \rangle$ , known as the McCauley parenthesis, is defined according to Eq. (5):

$$\langle x \rangle = \begin{cases} 0 & x \leq 0 \\ x & x > 0 \end{cases} \quad (5)$$

According to the definition of the operator  $\langle \rangle$ , if the normal strain assumes negative values, Eq. (4) is reduced to Eq. (6):

$$\gamma_{\text{shear}} = \sqrt{\gamma_{sn}^2 + \gamma_{tn}^2} \quad (6)$$

In order to separate the combined loading modes from single modes, if the normal strain is positive, the parameter  $\beta$  is defined as the mode combination ratio according to Eq. (7):

$$\beta = \frac{\gamma_{\text{shear}}}{\varepsilon_n} \quad (7)$$

In the present study, the sum of squared stresses was used as the criterion in order to predict the initiation location of interlayer debonding damage under the combined mode, which is presented in Eq. (8) [18]:

$$\left(\frac{\langle \sigma_n \rangle}{\sigma_n^0}\right)^2 + \left(\frac{\tau_{sn}}{\tau_{sn}^0}\right)^2 + \left(\frac{\tau_{tn}}{\tau_{tn}^0}\right)^2 = 1 \quad (8)$$

By combining Eq. (8) with Eqs. (2) to (7), the equivalent strain corresponding to the initiation location of interlayer debonding under combined mode is obtained according to Eq. (9):

$$\varepsilon_m^0 = \begin{cases} \varepsilon_n^0 \gamma^0 \sqrt{\frac{1 + \beta^2}{(\gamma^0)^2 + (\beta \varepsilon_n^0)^2}} \varepsilon_n < 0 \\ \gamma^0 \varepsilon_n \leq 0 \end{cases} \quad (9)$$

where  $\varepsilon_n^0$  and  $\gamma^0$ , respectively, represent the normal strains and out-of-plane shear strains at the damage initiation location in the interlayer element corresponding to the opening and pure shear modes, which are obtained according to Eq. (2).

Most criteria used in literature studies for prediction of interlayer debonding growth (complete interlayer damage) under combined loading mode are based on strain energy release rate and fracture toughness. In this study, the interlayer debonding growth was assessed using the well-known B-K criterion presented by Keane and Benzengagh [19].

The B-K criterion is obtained based on the fracture toughness in modes I and II, and additionally, in a general case and in the presence of all the three modes, the parameter  $\eta$ , which was obtained through Mixed-Mode Bending (MMB) experiment, are presented according to Eq. (10):

$$G_{lc} + (G_{uc} - G_{lc}) \left(\frac{G_{\text{shear}}}{G_T}\right)^\eta = G_c \quad (10)$$

$$G_T = G_l + G_{\text{shear}}$$

In this criterion, the toughness fracture is assumed to be equal in both pure shear modes III and II; however, since the fracture toughness of the former case is higher, a factor of safety is considered [15]. Moreover, since the cohesive zone element does not assume any differences between shear modes II and III, employing this criterion is reasonable.

By substituting Eqs. (3) to (7) into Eq. (10), the relationship between the effective strain corresponding

to the interlayer full debonding under combined loading is obtained according to Eq. (11) as:

$$\varepsilon_m^f = \begin{cases} \frac{2}{Kh_0 \varepsilon_m^0} \left[ G_{lc} + (G_{uc} - G_{lc}) \left(\frac{\beta^2}{1 + \beta^2}\right)^\eta \right] & \varepsilon_n > 0 \\ \gamma_m^f & \varepsilon_n < 0 \end{cases} \quad (11)$$

where  $\gamma_m^f$  is the shear strain at the end of the damage corresponding to the pure shear (slippage) mode  $\gamma_m^f$ , obtained using Eq. (3).

Among various factors, irreversibility of the damage parameter of the interlayer element should be of concern. To this end, a state variable which guarantees the maximum effective strain in any stage of loading is defined according to Eq. (12) [15]:

$$\varepsilon_k^* = \max\{\varepsilon_{k-1}^*, \varepsilon_m\} \quad (12)$$

where indices  $k$  and  $k-1$  are, respectively, the current and last loading steps. Moreover,  $\varepsilon_m$  is the current effective strain. The meaning of the state variable  $\varepsilon_m^*$ , as well as the damage parameter  $d$ , may be observed in Fig. 4.

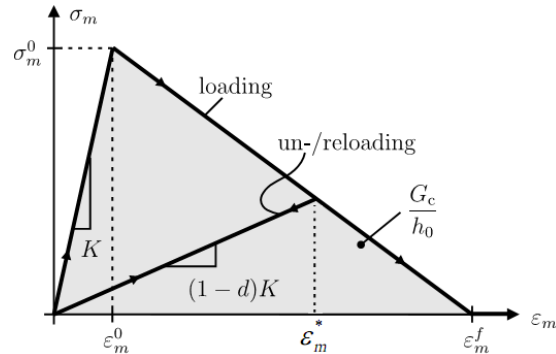


**Fig. 4.** Cohesive law for mixed-mode delamination with linear softening and maximum effective strain concept [15].

Based on the aforesaid explanations, the stress-strain relation in the structural equation is presented according to Eq. (13):

$$\sigma = C\varepsilon, \quad \sigma = \{\tau_{sn}, \tau_{tn}, \sigma_n\}^T, \quad \varepsilon = \{\gamma_{sn}, \gamma_{tn}, \varepsilon_n\}^T$$

$$C = \begin{cases} Kl\varepsilon_m^* \leq \varepsilon_m^0 \\ (1-d)KL + dKl\varepsilon_m^0 < \varepsilon_m^* < \varepsilon_m^f \\ Kl\varepsilon_m^* \geq \varepsilon_m^f \end{cases} \quad (13)$$

$$l_c = \begin{bmatrix} 0 & 0 & 0 \\ 0 & 0 & 0 \\ 0 & 0 & \frac{\langle -\varepsilon_n \rangle}{-\varepsilon_n} \end{bmatrix}$$

where  $C$  is the reduced interlayer stiffness matrix, and  $I$  is the identity matrix of order 3.

According to Fig. 4, the explicit relation of damage parameter for structural relations of the bilinear type under general combined mode is simply obtained using Eq. (14):

$$d = \frac{\varepsilon_m^f (\varepsilon_m^* - \varepsilon_m^0)}{\varepsilon_m^* (\varepsilon_m^f - \varepsilon_m^0)} \quad (14)$$

It should be noted that employing  $\varepsilon_m^*$  into Eqs. (13) and (14) meets the irreversibility condition associated with damage parameter in the interlayer element.

### 5.2. Determining the Model Constants under Static Loading

In order to assess the proposed approach, the static results reported by Chawla and Shen [7] were used because of the similarity between their materials and the present study's material.

As mentioned in Section 3, elastic behavior was considered in order to model the particles. Since silicon carbide was considered for the particles used in the present study, the required properties for which, e.g. Young's modulus and Poisson's ratio, are given in Table 1. Additionally, elastoplastic behavior was considered in order to model the metal matrix. The respective elastoplastic properties for the aluminum matrix under study are presented in Table 2.

In Table 2,  $E$  is Young's modulus,  $\nu$  is the Poisson's ratio, and  $S_y$  is the yield strength. Moreover,  $E_p$  represents the slope of the plastic region in the stress-strain graph obtained in the uniaxial tensile test for aluminum. As shown in Fig. 5, according to the behavior of the plastic region of the tested aluminum, linear approximation for the plastic region is convenient.

**Table 1**

Mechanical properties of SiC particle in Al-Cu-Mg (2080)/SiC composite [7].

E (GPa)	$\nu$
410	0.19

**Table 2**

Mechanical properties of Al matrix in Al-Cu-Mg (2080)/SiC composite [7].

E (GPa)	$\nu$	$S_y$ (MPa)	$E_p$ (MPa)
75	0.33	474	2033

However, the identification of CZM specifications associated with the particle-matrix inter-phase was carried out through matching the experimental results of silicon carbide reinforced aluminum matrix composite at a specific volume fraction. To this end, by considering plasticity behavior for the matrix with given constants (Table 2), the final properties of the inter-phase is obtained through trial and error in the software, such that the software-produced equivalent stress-strain diagram matches that of the experimental diagram for the

mentioned composite under displacement-controlled uniaxial tensile loading. For this purpose, first, the initial slope of the CZM graph is determined such that the initial slope of the software-produced graph which matches the experimental graph. Additionally, the strength of the CZM is selected such that the software-produced results on the initiation of stiffness decrease caused by damage matches the experimental diagram. Ultimately, the fracture toughness is obtained such that the rest of the stiffness decrease diagram caused by damage as well as the ultimate failure of the composite sample is predicted.

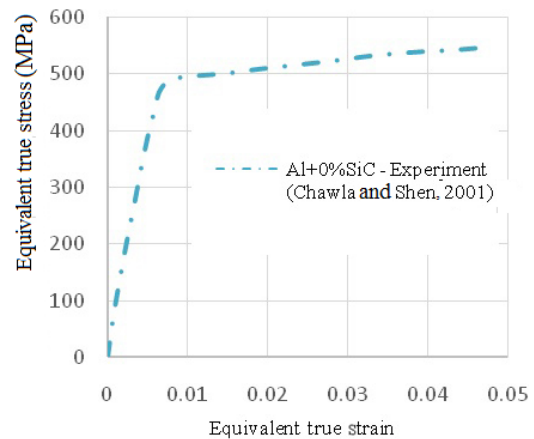


**Fig. 5.** Tensile behavior of an Al matrix in Al-Cu-Mg (2080)/SiC composite [7].

The described procedure was applied to a composite of 20 percent particle volume fraction with particle radii of 2.5 microns in ANSYS software package using the prepared code, and ultimately the properties were obtained according to Table (3). The interlayer element thickness was considered 0.0001 [20].

**Table 3**

Interface properties for cohesive zone model in Al-Cu-Mg (2080)/SiC composite.

K (GPa)	$\sigma_0$ (MPa)	$\tau_0$ (MPa)	$G_{lc}$ (N/mm)	$G_{llc}$ (N/mm)	$\eta$
75	1450	1450	0.15	0.15	1.0

Considering the isotropic nature of the matrix, it should be noted that the fracture toughness for modes I and II are equal, and the exponential parameter of B-K criterion is considered 1.

## 6. Fatigue Loading

### 6.1. Prediction of Fatigue Damage in the Matrix

During high-cycle loading and under small stresses, although plasticity may not occur, fatigue behavior adversely affects the elastic properties of the material. Hence, in order to appropriately predict the fatigue life of the composite, in addition to taking into account the

damage growth in the matrix-particle inter-phase, it is also necessary to consider fatigue damage growth in the matrix. To this end, considering the isotropic behavior of the matrix, its damage behavior may be described using a damage variable, which again describes the decline in Young's modulus as well as the shear modulus. This means that by defining the ratio of the decline in the stiffness to the initial stiffness in the current state as the damage variable, the reduced stiffness in a given state can be obtained using the following relation:

$$E_R = (1 - D)E_0, \quad G_R = (1 - D)G_0 \quad (15)$$

where  $E_0$  and  $G_0$  are the initial Young's and shear moduli of the matrix, respectively, and  $D$  is the damage parameter. This parameter represents the damage growth at a given point and may assume values between 0 and 1.

In order to predict the damage growth during fatigue loading, typically, the growth rate of the damage variable with respect to the load cycles is described based on loading parameters, i.e. stress, strain, and energy. In this study, it was assumed that the growth rate of the fatigue damage with respect to loading cycles  $N$  was governed by the following energy-based quasi-experimental relation [21]:

$$\frac{dD}{dN} = c \left( \frac{\Delta W^D}{W_0^D} \right)^m \quad (16)$$

where  $c$  and  $m$  are empirical constants, and  $\Delta W^D$  represents the changes in the strain (deformation) energy per unit volume of the sample in each loading cycle at the given integration point. The strain energy density is obtained through subtraction of the hydrostatic portion of the strain energy density from the total strain energy density.

The hydrostatic strain energy density is obtained using Eq. (17):

$$W^H = \frac{1}{2}\bar{\sigma}\varepsilon_{11}^* + \frac{1}{2}\bar{\sigma}\varepsilon_{22}^* + \frac{1}{2}\varepsilon_{33}^* \quad (17)$$

where  $\bar{\sigma}$  is the hydrostatic stress and  $\varepsilon_{ij}^*$  are its resulting strains. Hence:

$$\bar{\sigma} = \frac{(\sigma_{11} + \sigma_{22} + \sigma_{33})}{3}$$

$$\varepsilon_{ij}^* = \frac{(1 - 2\nu)\bar{\sigma}}{E}$$

consequently:

$$W^H = \frac{3(1 - 2\nu)\bar{\sigma}^2}{2E}$$

Moreover,  $W_0^D$  is the maximum strain energy density bearable by the material under uniaxial loading at the current moment, which is defined as Eq. (18):

$$W_0^D = \frac{(1 + \nu)}{3} \frac{(\sigma_{Ut}^R)^z}{E_R} \quad (18)$$

where  $\sigma_{Ut}^R$  is the residual strength at the current moment. Therefore, in order to determine the critical strain (deformation) energy density  $W_0^D$ , a criterion should be considered for residual strength. In the present study, it was assumed the residual strength is proportional to the residual stiffness. This is a valid assumption since the decrease in both stiffness and strength is associated with the increase in the damaged area in the concept of continuum damage mechanics. Additionally, considering such a valid assumption helps to reduce the parameters and required experiments for model specification. Therefore:

$$\sigma_{UT}^R = (1 - D)\sigma_{UT}^0 \quad (19)$$

The quantity  $W_0^D$  is then obtained according to Eq. (20):

$$W_0^D = \frac{(1 + \nu)}{3} (1 - D) \frac{(\sigma_{Ut}^0)^z}{E_0} \quad (20)$$

where  $\sigma_{Ut}^0$  is the initial tensile strength of the matrix. Ultimately, in order to determine the fracture time, a failure criterion should be employed. In this study, complete damage was considered as the corresponding density of critical distortion strain energy at a given time, which is also known as Von-Mises maximum distortion strain energy criterion. The critical Von-Mises stress is equal to the residual strength. As mentioned earlier, the considered criterion for matrix failure was also Von-Mises criterion, which is appropriate for ductile metals.

### 6.1.1. Specifications of the Matrix Constant under Specific Loading

The changes in strain energy under force-controlled cyclic loading with fixed maximum uniaxial stress  $\sigma_{11}$  and load ratio almost equal to zero is obtained according to Eq. (21).

$$W = \frac{(1 + \nu)}{3} \frac{(\sigma_{11})^2}{E_0(1 - D)} \quad (21)$$

By substituting Eq. (21) into Eq. (16), the growth rate of the fatigue damage is then obtained according to Eq. (22) as:

$$\frac{dD}{dN} = c \left( \frac{\sigma_{11}}{(1 - D)\sigma_{Ut}^0} \right)^{2m} \quad (22)$$

By integrating Eq. (22) with respect to the changes in the damage variable on the interval 0 to  $D$ , the following relation is achieved:

$$c \left( \frac{\sigma_{11}}{\sigma_{Ut}^0} \right)^{2m} N = \frac{1}{2m + 1} (1 - (1 - D)^{2m+1}) \quad (23)$$

The dimensionless stiffness after  $N$  cycles is calculated using Eq. (24):

$$\frac{E_R}{E_0} = \left( 1 - (2m - 1)c \left( \frac{\sigma_{11}}{\sigma_{Ut}^0} \right)^{2m} N \right)^{\left( \frac{1}{2m+1} \right)} \quad (24)$$

Here, considering the force-controlled loading at given stress  $\sigma_{11}$ , the fatigue life corresponds to the case where the residual strength reaches the applied stress. Hence, the ultimate value of the damage variable right before fracture in the sample is obtained using the following relation:

$$D^* = \frac{\sigma_{Ut} - \sigma_{11}}{\sigma_{Ut}} \quad (25)$$

Therefore, by substituting Eq. (25) into Eq. (23), the ultimate lifetime is determined using the following relation:

$$N_f = \frac{\left( 1 - \left( \frac{\sigma_{11}}{\sigma_{Ut}^0} \right)^{2m+1} \right)}{(2m + 1)c \left( \frac{\sigma_{11}}{\sigma_{Ut}^0} \right)^{2m}} \quad (26)$$

By comparing Eqs. (24) and (26), Eq. (27) is achieved, which describes the relation between dimensionless loading cycles and dimensionless Young's modulus under tensile loading:

$$\frac{N}{N_f} = \frac{\left( 1 - \left( \frac{E_R}{E_0} \right)^{2m+1} \right)}{\left( 1 - \left( \frac{\sigma_{11}}{\sigma_{Ut}^0} \right)^{2m+1} \right)} \quad (27)$$

Therefore, having the fatigue results associated with the stress-life or stiffness decrease with respect to loading cycles under pure tensile strength for the considered material, the model constants can be determined using Eqs. (26) and (27).

To this end, with regards to the stress-life diagram for the aluminum presented in the study of Chawla and Shen (2001), applying curve-fitting on the stress-life results as well as the life relation as a function of stress (Eq. 26), the constants related to matrix fatigue were obtained as 0.00013 and 3 for the coefficient  $c$  and exponent  $m$  in the relation of matrix fatigue damage growth rate. Note that the ultimate strength of the mentioned aluminum was 548MPa.

## 6.2. Simulation of Particle-matrix Debonding

In Sections 4 and 5, CZM was introduced in order to predict the particle-matrix debonding failure mode during static loading. In this section, aiming at growth prediction of the aforementioned damage under cyclic

loading, the appropriate, complementary structural equations based on continuum damage mechanics are presented. In this approach, the growth rate of the damage in the particle-matrix interphase with respect to the fatigue loading cycles is based on a structural equation. Evidently, under high-cycle loading, damage and consequently crack growth are caused by periodic loadings applied at a high number of cycles. Hence, regarding the complex nature of fatigue damage, it is necessary to derive the model constants based on appropriate fatigue experiments so as to validate the model for different samples.

Generally, the proposed models regarding this subject are categorized into two general groups:

Group 1: The models in which the fatigue damage growth is considered fully independent and is according to the framework of damage mechanics based on appropriate assumptions [22, 23].

Group 2: The models which relate the fracture mechanics, specifically Paris' law, to damage mechanics in order to formulate the fatigue growth rate in cohesive element [24, 25].

Since models based on damage mechanics provide more accurate estimations of the damage growth due to their more accurate physical model, the present study decided to use them, specifically the model proposed by Turon et al., in order to simulate the damage growth in the interphase of metal matrix composites [27].

### 6.2.1. The Structural Relations for Cohesive Element

In addition to interlayer strength and fracture toughness, the initial stiffness of the structural relation, as well as the length of the cohesive zone, are among the most influential parameters affecting the behavior of the interlayer element. So far, various approaches have been proposed for selecting the initial stiffness of the interlayer element, among which Daudeville et al. [26] described the stiffness in the stress-displacement space based on the thickness of the interlayer element according to Eq. (28):

$$K_n = \frac{E_n}{h_0}, \quad K_{sn} = \frac{2G_{sn}}{h_0}, \quad K_{tn} = \frac{2G_{th}}{h_0} \quad (28)$$

where  $E$  and  $G$  are elastic stiffness of the rich resin zone, which may be assumed equal to that of the homogeneous layer.

In order to accurately assess the interlayer debonding growth, a sufficient number of interlayers should exist along the length of the cohesive zone around the crack tip. Hence, in order to achieve the optimal number of required elements for modeling, it is necessary to determine the length of the cohesive zone, which is the distance from the crack tip to the point with maximum cohesive stress, along with the minimum number of interlayer elements in this zone. Moreover, an accurate

estimation of this parameter is highly important in the appropriate prediction of interlayer debonding caused by high-cycle loading [26]. To this end, Turon et al. conducted a comprehensive study on the length of the cohesive zone, according to the results of which various analytical solutions exist for estimating the length of the cohesive zone under fully developed conditions in different samples. However, the structure of all these relations are similar and are only different in a coefficient. This relation is in the form of Eq. (29) [26]:

$$l_{cz} = (M)E_m \frac{G_c}{(\tau_c)^2} \quad (29)$$

In Eq. (29),  $E$  is Young's modulus along the thickness direction,  $G_c$  is the fracture toughness, and  $\tau_c$  is the strength of the interlayer zone. Additionally, parameter  $M$  assumes different values for different models of the cohesive zone. For instance, Bao and Sou obtained 0.73 for the bilinear cohesive zone model [28].

It should be noted that Turon et al. [24] substituted the relation for the length of the cohesive zone with the analytical solution proposed by Rice [29]. Rice's estimation is based on the assumption that stress linearly varies with the distance from the crack tip within the cohesive zone. Numerical results reveal that this assumption does not hold true. The length of the cohesive zone obtained by Bao and Suo [28] was calculated for the bilinear CZM, which is in agreement with the employed CZM model of this study.

Hence, in the present study, the length parameter of the cohesive zone in relations was considered according to the solution of Bao and Sou as the following Eq. [28]:

$$l_{cz} = 0.732 \frac{E_m G_c}{(\tau_0)^2} \quad (30)$$

Regarding the length of the cohesive zone under fully developed conditions, it should be noted that it is considered the length at which the strain energy release rate of the crack approaches the fracture toughness of the materials, meaning that the crack tip is fully damaged and is on the verge of growing.

Obviously, the crack area growth rate in a standard sample with a fixed width can be described with respect to the crack length growth rate according to Eq. (31):

$$\frac{dA}{dN} = b \frac{da}{dN} = bc \left( \frac{\Delta G}{G_c} \right)^m \quad (31)$$

where  $m$  and  $c$  are the constants in Paris' law for crack length growth rate,  $b$  is the length of the crack front (width of the sample),  $\Delta G$  is the changes in the strain energy release rate of the cohesive element during the current fatigue cycle, the concept of which is demonstrated in Fig. 6, and  $G_c$  is the fracture toughness, i.e. the total area bounded by the graph of cohesive zone.

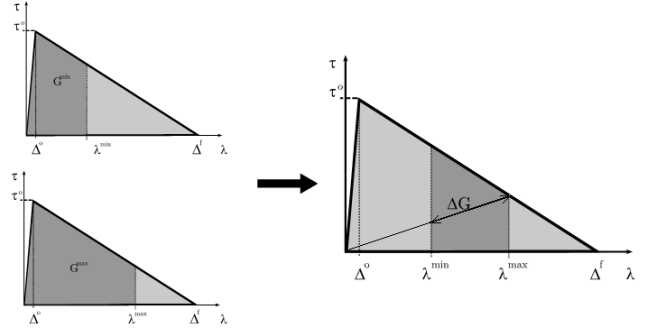


**Fig. 6.** Changes in the strain energy release rate of the cohesive zone element during the fatigue cycle [25].

In order to relate the crack area growth rate with the damage growth rate, Turon et al. proposed a concept known as *damaged area*, which is a function of element damage variable and its associated elements in the cohesive zone. According to Eq. (32), it was assumed that the growth rate of the damaged area during fatigue loading is similar to the crack area growth rate in Paris' law, and is hence a function of strain energy release rate of the cohesive element during the fatigue cycle:

$$\frac{\partial A_d}{\partial N} = A_\varepsilon \left[ \frac{C}{l_{cz}} \left( \frac{\Delta G}{G_c} \right)^m \right] \quad (32)$$

where  $A_d$  is the damaged area of the element,  $A_\varepsilon$  is the cohesive element area in the interlayer debonding plane, and  $l_{cz}$  is the length of the formed cohesive zone normal to the crack front.

According to the abovementioned relation, if the damaged area of the element ( $A_d$ ) is appropriately defined so that the proposed quasi-Paris' law holds true, the damage variable growth rate during fatigue loading may be calculated for the cohesive element using the following relation:

$$\frac{\partial d}{\partial N} = \frac{\partial d}{\partial A_d} \frac{\partial A_d}{\partial N} \quad (33)$$

However, it is still necessary to deal with the relation for the damaged area in the cohesive element. Additionally, Turon et al. used the concept of (irreversible) dissipated energy. They assumed the ratio of the damaged area of the element to the total area of the element at each state of damage variable is equal to the ratio of the dissipated energy  $\Xi$  during the damage process to the critical energy release rate  $G_c$  [28]. This is demonstrated in Fig. 7. Hence, we may write:

$$\begin{aligned} A_d &= A_\varepsilon \frac{\Xi}{G_c} = A_\varepsilon \left[ \frac{1 - (G_c - \Xi)}{G_c} \right] \\ &= A_\varepsilon \left[ \frac{1 - \tau \varepsilon_m^*}{\tau_m^0} \right] \end{aligned} \quad (34)$$

Where  $\varepsilon_m^*$  is the maximum effective strain during each loading stage.

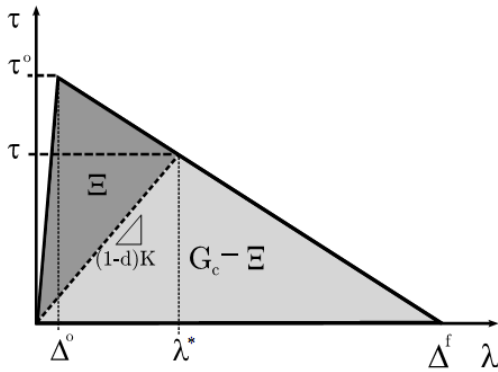


**Fig. 7.** The concept of dissipated energy in linear softening rule [25].

By substituting the stress-strain relation into Eq. (34), and by calculating  $\varepsilon^*$  with respect to damage variable  $d$  using Eq. (14), the final relation for the damaged area with respect to the element damage variable is obtained according to Eq. (35):

$$A_d = A_\epsilon \left[ \frac{d\varepsilon_m^0}{(1-d)\varepsilon_m^f + d\varepsilon_m^0} \right] \quad (35)$$

As shown, in case of  $d$  assumes zero, the damaged area is also zero, and as  $d$  approaches 1, the damaged area equals the element area.

By differentiating the recent relation, it can be proved that the growth rate of the damage variable  $d$  with respect to the damaged area is obtained as:

$$\frac{\partial d}{\partial A_d} = \frac{1}{\partial A_d} = \frac{1}{A_\epsilon} \frac{[(1-d)\varepsilon_m^f + d\varepsilon_m^0]^2}{\varepsilon_m^f \varepsilon_m^0} \quad (36)$$

By substituting Eqs. (32) to (36) in Eq. (33), the growth rate of the damage variable in the cohesive element under fatigue loading may be calculated as:

$$\frac{\partial d}{\partial N} = \quad (37)$$

$$\begin{cases} \frac{[(1-d)\varepsilon_m^f + d\varepsilon_m^0]^2}{\varepsilon_m^f \varepsilon_m^0} \left[ \frac{C}{l_{cz}} \left( \frac{\Delta G}{G_C} \right)^m \right] & \text{for } G_{\max} \geq G_{th} \\ 0 & \text{otherwise} \end{cases}$$

where  $G_{th}$  is the strain energy release rate of the cohesive element on the verge of fatigue initiation, and  $C$  and  $m$  are the Paris' law constants obtained through fatigue experiments conducted on standard samples or through the software adjustment under special conditions.

### 6.2.2. Determining the Model Constants under Fatigue Loading

In order to determine the fatigue constants associated with the particle-matrix interphase, the stress-life

results for an aluminum matrix composite reinforced with 20 percent volume fraction SiC particles were obtained at three stress levels. Then, the constants  $c$  and  $m$  in the relation of fatigue damage growth for the particle-matrix interphase were obtained through software trial and error so that the experimentally obtained fatigue life is predicted by software analysis for the mentioned three stress levels, which were considered 240, 280, and 300MPa. The experimentally obtained average fatigue lives for these three stress levels were 3350000, 150000, and 60000 cycles, respectively [7].

According to described procedure, the trial and error was carried out and the exponent constant  $m$ , as well as the coefficient constant  $c$  in the relation of fatigue damage growth rate, were obtained as 3.5 and 3.15mm/cycle, respectively.

## 7. The Results of FEM Analysis

### 7.1. Ecstatic Loading

Using the relations obtained in Section 5, the stress-displacement diagram of the structural equation for the considered material is presented in Fig. 8.

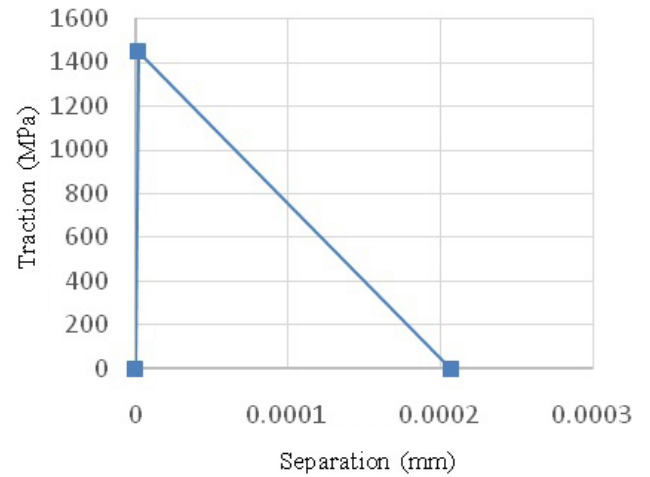


**Fig. 8.** Interface phase traction and separation of Al-Cu-Mg (2080)/ SiCp composite.

In Fig. 9, the numerical results of equivalent stress-strain diagram for the considered composite with the given properties of Table 3 are presented along with the experimental results.

As shown in Fig. 9, the presented constants of Table 3 appropriately fit the experimental results. Moreover, the implemented model was able to appropriately predict the ultimate failure in the part. Correct prediction of the mechanical behavior of the metal matrix composite is not possible without taking into account the interphase damage. Figs. 10 and 11, respectively, illustrate the gradual growth of the equivalent plastic strain in the matrix and the damage growth in the matrix-particle interphase.

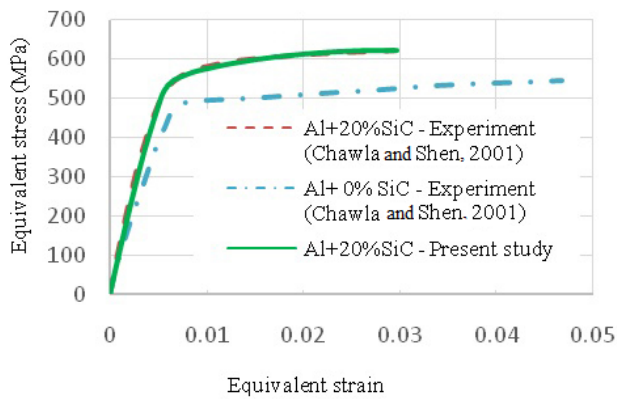


**Fig. 9.** Tensile behavior of an Al-Cu-Mg (2080)/ SiCp composite with particle volume fraction 20%.

As demonstrated in Figs. 10 and 11, first, plasticity in the matrix occurs at the connection of the middle particle with the matrix, and as the plastic strain grows in the matrix, the damage is initiated in the interphase of the same particle-matrix location along the loading

direction and continues. This is in good agreement with experimental results [20].

Damage initiation along the loading direction is reasonable in physical terms considering the formation of the debonding mode. It should be noted that the damage in the interphase indicates crack growth between the particle and matrix.

In order to validate the performance of the proposed method in predicting other circumstances, using the same material constants presented in Section 5, the same composite but with a particle volume fraction of 10 percent was numerically analyzed, the results of which are presented in Fig. 12.

In order to assess the sensitivity of the model and the considered composite to their material parameters, the results of equivalent stress-strain diagram for the considered composite with 20 percent particle volume fraction at different interlayer strength and fracture toughness of the interphase are demonstrated in Fig. 13.

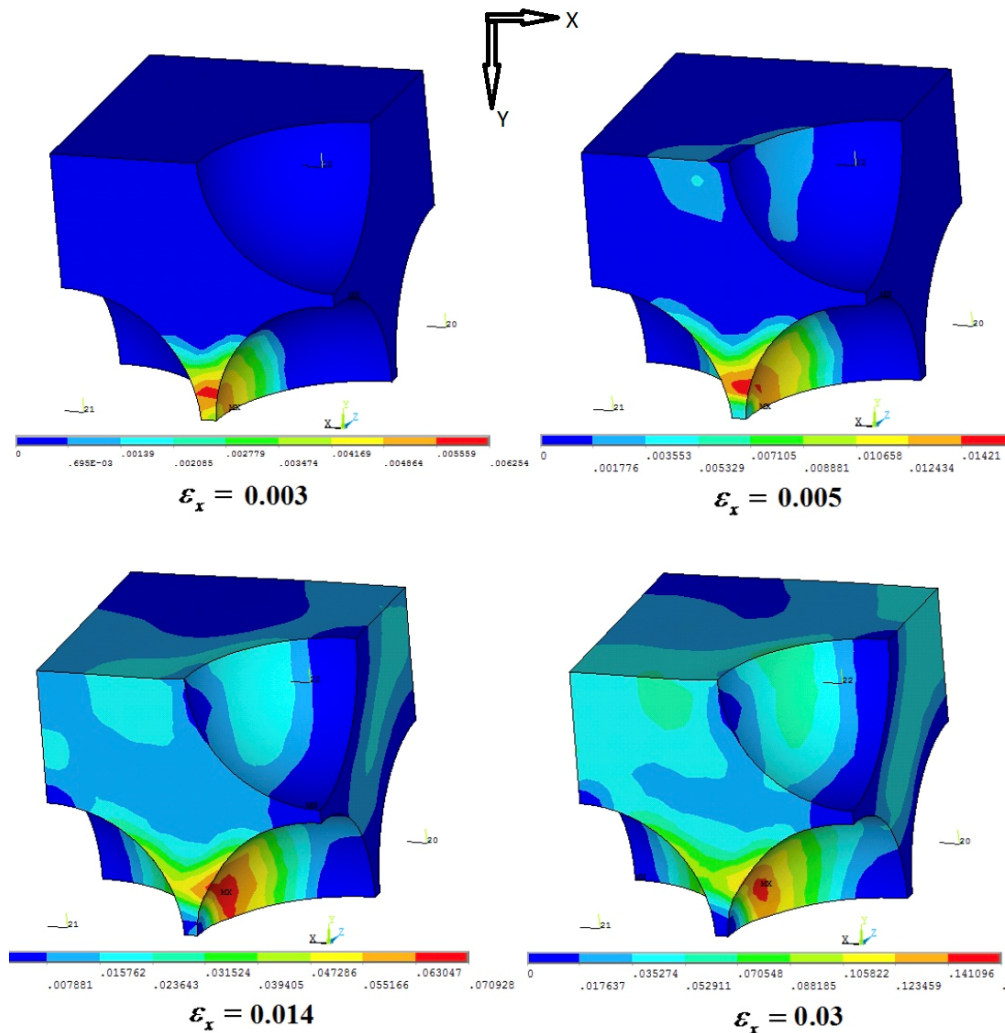


**Fig. 10.** The results of the gradual growth of equivalent plastic strain in the matrix for aluminum matrix composite with 20% volume fraction reinforcement SiC particles under uniaxial stress.

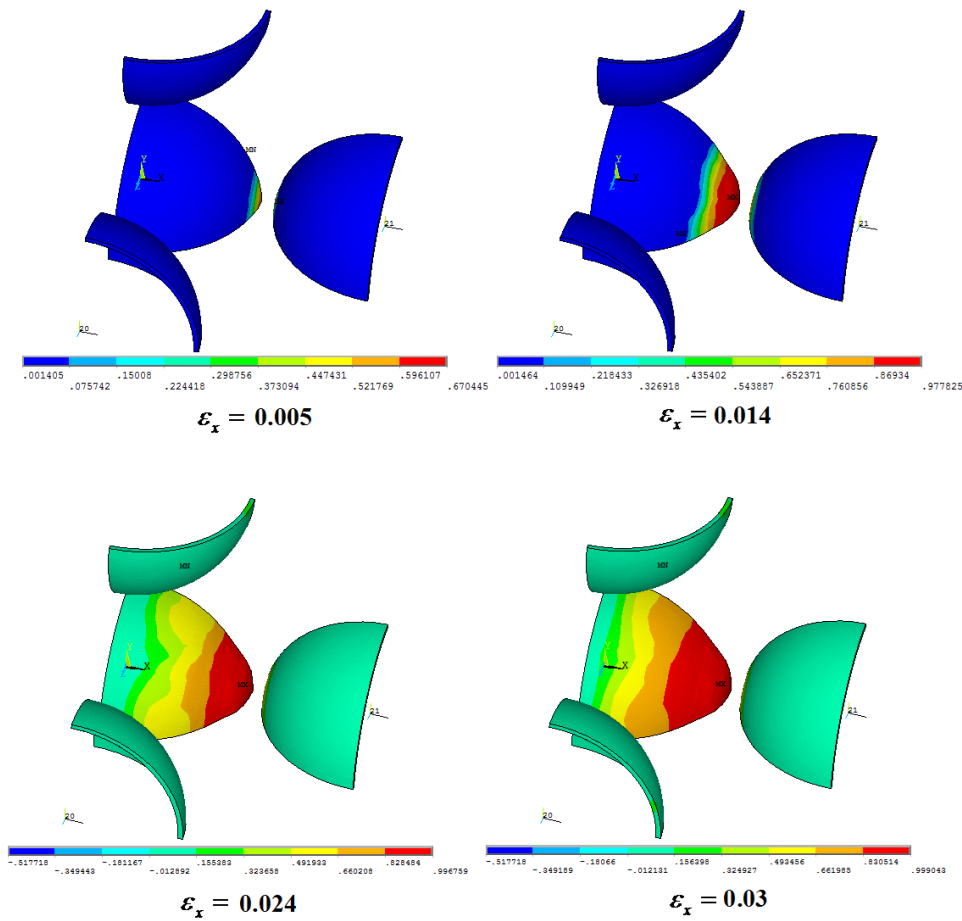


**Fig. 11.** The results of the gradual growth of damage in matrix and particle interface phase for aluminum matrix composite with 20% volume fraction reinforcement SiC particles under uniaxial stress.

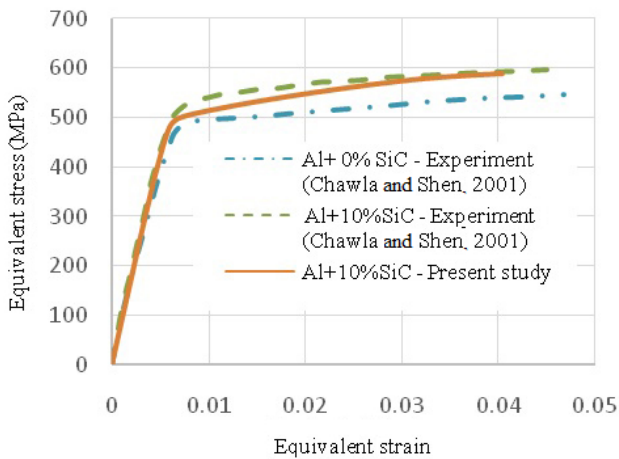


**Fig. 12.** Tensile behavior of an Al-Cu-Mg (2080)/SiCp composite with particle volume fraction 10%.

Regarding the effect of particle sizes on these properties, this analysis somehow demonstrates the effect of particle sizes on the results. According to the studies of Chawla and Shen [7], increasing the particle sizes at a fixed volume fraction leads to a decrease in the strength as well as fracture energy of the composite. This effect is predictable as the interlayer strength and

fracture toughness is decreased.

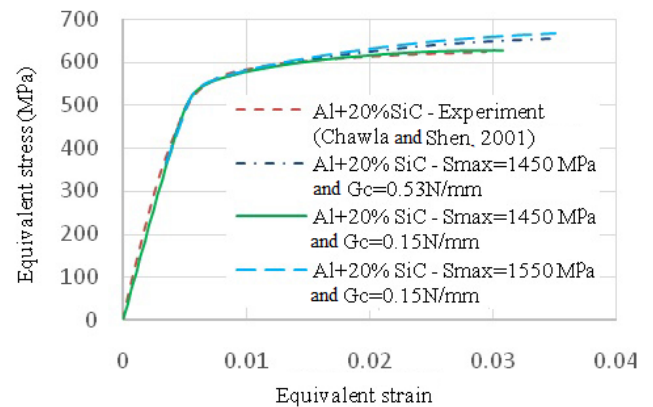


**Fig. 13.** Evaluate the effect of physical parameters on the results of a static diagram stress-strain for 20% volume fraction.

As shown in Fig. 13, as the interlayer fracture toughness and strength increases, the damage in the sample is slowed down, causing an upward shift in the diagram. Additionally, the ultimate strength of the sample is increased. Note that according to this figure, the model is more sensitive to the interlayer strength.

### 7.2. Fatigue Loading

According to the explanations given in Section 6.1.1, the constants associated with fatigue damage growth in the matrix are obtained using the results of a fatigue test on the pure matrix subject to uniaxial tensile fatigue loading. In Fig. 14, the prediction results of the proposed model, as well as the experimental results, are presented.

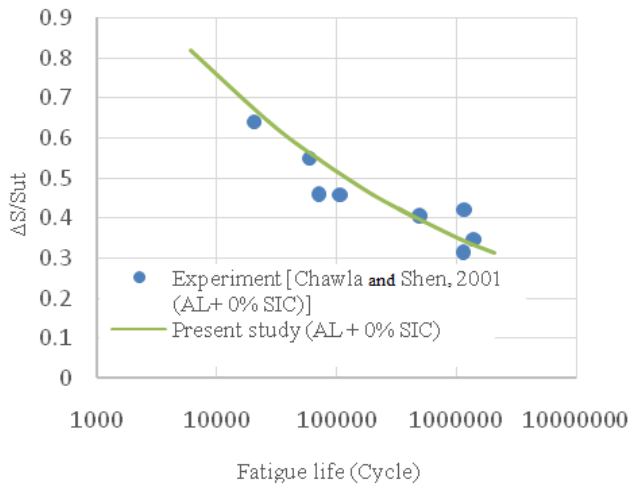


**Fig. 14.** The fatigue stress-life diagram of the uniaxial tensile test on the aluminum matrix.

As demonstrated in Fig. 14, the considered model is able to appropriately simulate the experimental behavior of fatigue damage growth.

In this section, in order to validate the model under fatigue loading, the predicted fatigue life results by software analysis are compared to experimental results at other stress levels as well as another volume fraction (10 percent). The comparison results are presented in Fig. 15 and 16.

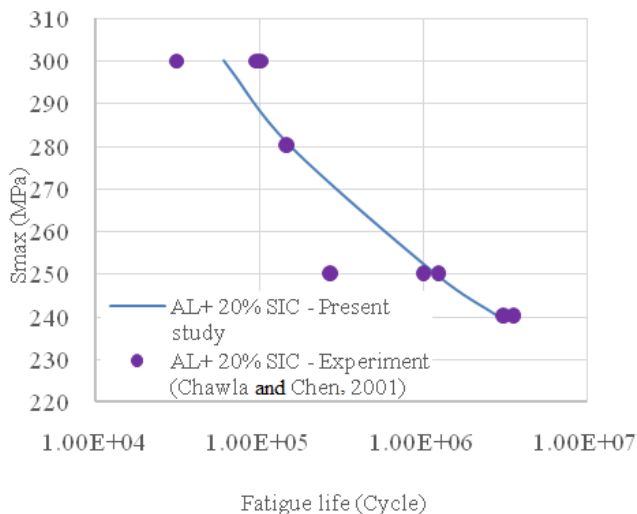


**Fig. 15.** Comparison of the fatigue life results obtained through software prediction and experimental results for a sample with 20 percent particle volume fraction.

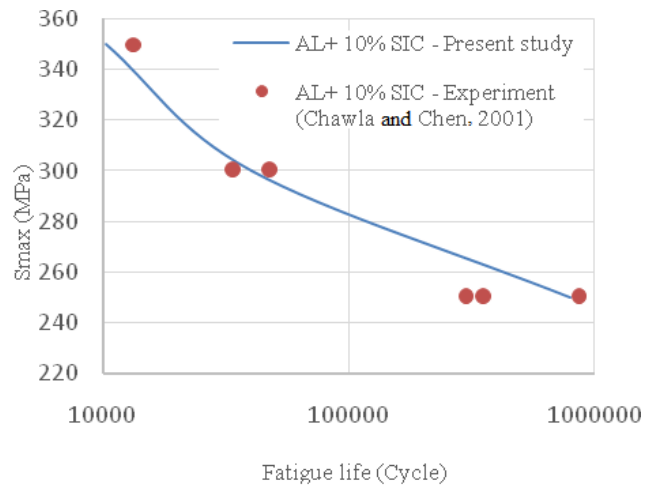


**Fig. 16.** Comparison of the fatigue life results obtained through software prediction and experimental results for a sample with 10 percent particle volume fraction.

The particles volume fraction is one of the important parameters regarding PMMCs as it significantly affects the strength and fatigue behavior of the composite. In this section, in order to assess the performance of the implemented model, the effect of particle volume fraction in the prediction of fatigue life is compared for two cases where 10 and 20 percent particle volume fractions are used. The comparison results are presented in Fig. 17.

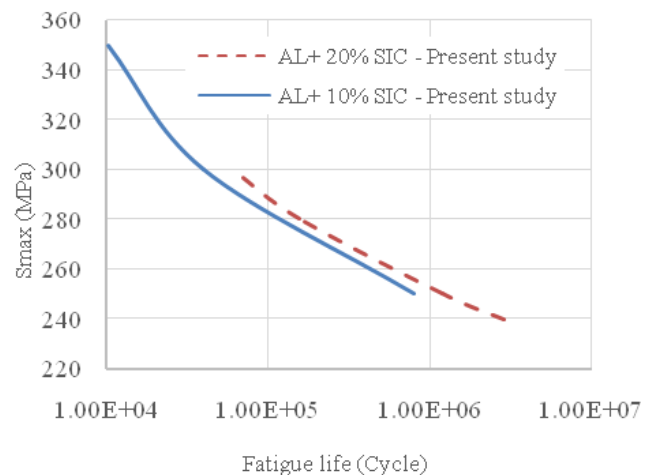


**Fig. 17.** Comparing the effect of particle volume fraction in predicting the fatigue life using the implemented model.

As shown, by increasing the particle volume fraction from 10 to 20 percent, the fatigue life of the metal matrix composite at a fixed maximum stress level is increased. This is in agreement with experimental results [7].

Hence, the implemented model is appropriately capable of taking into account the effect of particles volume fraction in the prediction of fatigue life.

## 8. Conclusions and Results

In the present study, the fatigue life of PMMCs was investigated using a micromechanical modeling approach. To this end, a representative volume element of the composite with its respective volume fraction was considered, which included three components; namely the matrix, the particle, and the inter-phase between particles. In order to more accurately predict the behavior of damage growth in the considered composite, the inter-phase was modeled using the cohesive zone model (CZM), and the matrix behavior was modeled using destructive elastoplastic behavior. In order to model the behavior of damage growth in the inter-phase, a powerful model for fatigue damage growth, the performance of which was previously validated for multilayer composites, was implemented through the material code written in the subroutine (User mat) of ANSYS software package. Moreover, the behavior of fatigue damage growth in the matrix was implemented in ANSYS using an energy-based model using the User mat subroutine. It should be noted that the mentioned micromechanical approach was first used for the prediction of fatigue damage growth in metal matrix composites.

Then, in order to assess the performance of the implemented model, the fatigue damage growth in an aluminum matrix composite reinforced with SiC particles was investigated. To this end, in order to determine the static constants of the implemented cohesive model, the results of static uniaxial tensile loading on the mentioned composite with 20 percent particle volume fraction was used. Then, the static part of the model was validated through predicting the behavior of static damage growth of the composite with 10 percent particle volume fraction.

To determine the fatigue constants of the matrix, the experimental results of stress-fatigue life diagram for pure aluminum were used, through which the respective constants were derived. Then, the fatigue constants of CZM associated with damage growth in the interphase were derived through the stress-fatigue life results of the composite with 20 percent particle volume fraction at three different stress levels.

Ultimately, in order to validate the performance of the model in fatigue life prediction of PMMCs under other conditions, the fatigue life was investigated for different stress levels and another particle volume fraction. The results were then compared with the corresponding experimental results.

Although the implemented model uses similar material constants for the interphase at different particle volume fractions, it is able to predict different results for different particle volume fractions. For instance, increasing volume fraction from 10 to 20 percent increases the composite strength, while decreasing the growth in length. This is also confirmed by experimen-

tal results [7]. Hence, the effects of volume fraction can be easily observed on the results of the model.

Analysis of the model results with respect to model parameters revealed that the CZM is more sensitive to the parameter of interlayer strength. Hence, utmost care must be taken in determining this constant.

Although the model employed a few tests in determining the constant models, the results indicate it was also able to appropriately predict the fatigue life of PMMCs under other conditions. The results obtained from numerical simulations indicate that the proposed model is capable of taking into account the effects of volume fraction in predicting fatigue life. Hence, one of the important features of the model is its ability to take into account the effects of volume fraction in the prediction of fatigue life.

## References

- [1] W.F. Smith, *Structure and Properties of Engineering Alloys*, Lubbock, TX, USA: McGraw-Hill, (1981).
- [2] S. Attar, M. Nagaral, H.N. Reddappa, V. Auradi, A review on particulate reinforced aluminum metal matrix composites, *J. Emerging Tech. Innovative Res.*, 2(2) (2015) 225-229.
- [3] A. Shokuhfar, M. Sabzehparvar, F. Kiani, *The Science and Engineering of Advanced Materials Smart and Nanostructured Materials*, Tehran, Iran: kntu publication, (2014) (In Persian).
- [4] H. Abdollah pours, *Metal Matrix Composites*, Semnan, Iran: Semnan University Press, (2013) (In Persian).
- [5] C. Kaynak, S. Boylu, Effects of SiC particulates on the fatigue behaviour of an Al-Alloy matrix composite, *Mater. Des.*, 27(9) (2006) 776-782.
- [6] N. Chawla, K.K. Chawla, *Metal Matrix Composites*, First Edition: Springer US Publisher, (2006).
- [7] N. Chawla, Y.L. Shen, Mechanical behavior of particle reinforced metal matrix composites, *Advanced Engineering Materials*, 3(6) (2001) 357-370.
- [8] N. Chawla, J.E. Allison, *Fatigue of Particle Reinforced Materials*, In *Encyclopedia of Materials: Science and Technology*, Second Edition, Elsevier Amsterdam, The Netherland, (2001) 2967-2971.
- [9] J.J. Lewandowski, *Fracture and Fatigue of Particulate MMCs*, In: T.W. Clayne (ed.), *Compr. Compos. Mater. Metall. Matrix. Compos.*, Elsevier, 3 (2000) 151-187.
- [10] J. LLorca, *Fatigue of particle and whisker reinforced metal matrix composites*, *Prog. Mater. Sci.*, 47(3) (2002) 283-353.

- [11] V.V. Ganesh, N. Chawla, Effect of reinforcement-particle-orientation anisotropy on the tensile and fatigue behavior of metal-matrix composites, *Metall. Mater. Trans. A*, 35(1) (2004) 53-61.
- [12] J. Nemati, S. Sulaiman, A. Khalkhali, Improvement in mechanical properties of titanium deformed by ECAE process, *J. Stress Anal.*, 1(1) (2016) 55-64.
- [13] A. Madadi, H. Eskandari-Naddaf, M. Nemati-Nejad, Evaluation of bond strength of reinforcement in concrete containing fibers, micro-silica and nano-silica, *J. Stress Anal.*, 3(1) (2018) 11-19.
- [14] G.H. Majzoubi, K. Rahmani, A. Atrian, An experimental investigation into wear resistance of Mg-SiC nanocomposite produced at high rate of compaction, *J. Stress Anal.*, 3(1) (2018) 35-45.
- [15] C. Balzani, W. Wagner, An interface element for the simulation of delamination in unidirectional fiber-reinforced composite laminates, *Eng. Fract. Mech.*, 75(9) (2008) 2597-2615.
- [16] P.P. Camanho, C.G. Davila, M.F. De Moura, Numerical Simulation of Mixed-Mode Progressive Delamination in Composite Materials, *J. Compos. Mater.*, 37(16) (2003) 1415-1438.
- [17] S. Sridharan, *Delamination Behavior of Composites*, Boca Raton, Woodhead Publisher, USA: CRC Press, (2008).
- [18] L. Ye, Role of matrix resin in delamination onset and growth in composite laminates, *Compos. Sci. Technol.*, 33(4) (1988) 257-277.
- [19] M.L. Benzeggagh, M. Kenane, Measurement of mixed-mode delamination fracture toughness of unidirectional glass/epoxy composites with mixed-mode bending apparatus, *Compos. Sci. Technol.*, 56(4) (1996) 439-449.
- [20] Q. Meng, Z. Wang, Prediction of interfacial strength and failure mechanisms in particle-reinforced metal-matrix composites based on a micromechanical model, *Eng. Fract. Mech.*, 142 (2015) 170-183.
- [21] D. Salimi-Majd, Investigation of delamination in laminated composites under fatigue loading using the cohesive interface element, MSc Thesis, School of mechanical engineering, Iran University of Science and Technology, Tehran, (2013) (In Persian).
- [22] P. Robinson, U. Galvanetto, D. Tumino, G. Bellucci, D. Violeau, Numerical simulation of fatigue-driven delamination using interface elements, *Int. J. Numer. Methods Eng.*, 63(13) (2005) 1824-1848.
- [23] H. Khoramishada, A.D. Crocombe, K.B. Katnana, I.A. Ashcroft, A generalised damage model for constant amplitude fatigue loading of adhesively bonded joints, *Int. J. Adhes. Adhes.*, 30(6) (2010) 513-521.
- [24] A. Turon, J. Costa, P.P. Camanho, C.G. Dávila, Simulation of delamination in composites under high-cycle fatigue, *Compos. Part A*, 38(11) (2007) 2270-2282.
- [25] A. Pirondi, F. Moroni, A progressive damage model for the prediction of fatigue crack growth in bonded joints, *J. Adhes.*, 86(5-6) (2010) 501-521.
- [26] L. Daudeville, O. Allix, P. Ladevèze, Delamination analysis by damage mechanics: Some applications, *Compos. Eng.*, 5(1) (1995) 17-24.
- [27] A. Turon, J. Costa, P.P. Camanho, P. Maimí, Analytical and Numerical Investigation of the Length of the Cohesive Zone in Delaminated Composite Materials, In: *Mechanical Response of Composites*, Computational Methods in Applied Sciences, Springer, Dordrecht publisher, (2008).
- [28] G. Bao, Z. Suo, Remarks on crack-bridging concepts, *Appl. Mech. Rev.*, 45(8) (1992) 355-366.
- [29] J.R. Rice, The Mechanics of Earthquake Rupture, In: A.M. Dziewonski, E. Boschi, (eds.) in *Physics of the Earth's Interior (Proc. International School of Physics 'Enrico Fermi', Course 78, 1979)*, Italian Physical Society and North-Holland Publisher Co., (1980) 555-649.